13th ewtec 2019 Proceedings of the 13th European Wave and Tidal Energy Conference 1-6 Sept 2019, Naples, Italy

# A floating/submersible shrouded tidal current turbine system applicable in low speed tidal flow

Yusaku Kyozuka, Daisaku Sakaguchi, Makoto Sueyoshi and Changhong Hu

*Abstract*—**Research and development of a low cost floating/submersible type tidal current turbine system which can be used in low speed tidal currents is introduced. The system consists a horizontal axis turbine power generator with a shroud or diffuser and a slack mooring system using four ropes. The shroud provides buoyancy so that the tidal current turbine floats to the surface when the tidal current is low but it submerges midstream (vertically) to generate power when the tidal current exceeds a certain speed. An optimum shape of the shroud and the turbine was obtained using a Genetic Algorithm optimization system. The tidal current turbine moored by the ropes changes its direction passively according to the direction of the tidal current. Results of the model experiments in a circulating water channel and a towing tank are reported to show the performance of the system. A sea trial of a 5kW larger scale model is planned in near future.**

*Keywords*—**Tidal current power generator, optimized design using Genetic Algorithm, floating/submersible turbine, large diffuser, rope mooring.**

## I. INTRODUCTION

Tidal current power generation is already in the early stages of commercial use and demonstration experiments are being carried out at several places around the world, with large turbines up to megawatt capacities. Such an increase in turbine size is necessary to lower the power generation cost, but a fast current is necessary for this capability, and the sea area for such turbines is quite limited in Japan. On the other hand, since the tidal current energy is stable and predictable, it could be an attractive alternative power source for isolated islands that have to rely on independent power supplies (mainly diesel generators).

We propose a low cost yet high-performance power generator that can be used in low speed tidal currents. We adopted a floating/submersible tidal current power system which consists of a high-performance power generator that can be used in tidal flow speed conditions up to 3 knots (1.5 m/s) for example, and uses 4 mooring ropes to minimize installation and recovery cost (OPEX). Unlike wind, the maximum velocity of tidal current can be predicted quite accurately, so the cut-out flow velocity can be chosen slightly larger than the maximum flow velocity. In this system, when the tidal current velocity is low, the power generator floats to the water surface, and when the tidal current velocity is equal or greater than a certain level, it goes under the water passively and generates electricity in the tidal current. Maintenance is conducted using a small boat such as a fishing boat when the tidal current is low. Since the generator is floating on the surface, it is easy to tow to port without expensive marine work, thus making it possible to reduce the maintenance costs significantly. Results of tank tests using a 1/6 scale model prototype turbine are presented.

## II. TIDAL POWER POTENTIAL MAP IN NAGASAKI WATERS

In order implement tidal current power generation, it is necessary to locate the optimum location for a specific generator within the available area/s. For this purpose, tidal simulation is required, but detailed bathymetry data of the target area/s is necessary to obtain accurate results.

However, at present, apart from 500 m resolution mesh data provide by the Japan Ocean Data Centre (JODC), there is no detailed data for specific sea areas around Japan. Therefore, in this study, we generated bathymetry data from nautical maps within the areas shown in Fig. 1 and conducted tidal simulations to obtain tidal current potential maps within the Nagasaki waters.

The red frames in Fig. 1 show the waters where 10 m mesh (min.) detailed data sets were generated. Fig.2 shows a 75-day sample of tidal current simulation near Tsushima. Based on this data we can ascertain that the maximum tidal speed at spring tide is 1.8 m/s. Since Tsushima is a remote island and relies on independent

ID 1539 track TDD

Y. Kyozuka is with the Organization for Marine Science and Technology, Nagasaki University, 1-14 Bunkyo-Machi, Nagasaki, Japan 852-8521 (e-mail: kyozuka@nagasaki-u.ac.jp).

D. Sakaguchi is with the Faculty of Engineering, Nagasaki University, 1-14 Bunkyo-Machi Nagasaki, Japan 852-8521 (e-mail: daisaku@nagasaki-u.ac.jp).

M. Sueyoshi is with the Research Institute for Applied Mechanics, Kyushu University, 6-1 Kasuga-Koen, Kasuga, Japan 816-8580 (e-mail: sueyoshi@riam.kyushu-u.ac.jp).

C. Hu is with the Research Institute for Applied Mechanics, Kyushu University, 6-1 Kasuga-Koen, Kasuga, Japan 816-8580 (e-mail: hu@riam.kyushu-u.ac.jp).

  

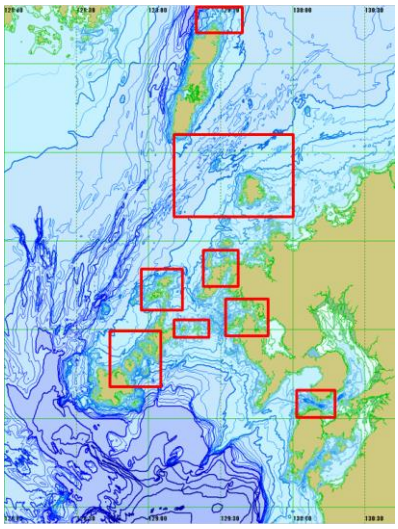

Fig. 1. Eight candidate sea areas for tidal current power generation in Nagasaki.

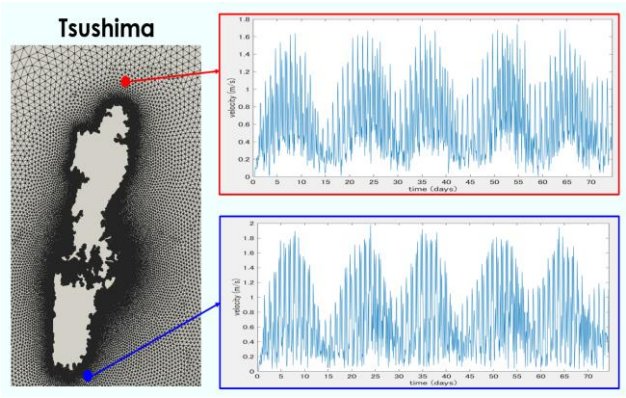


Fig. 2. Tidal current speed of the points near Tsushima for 75 days.

electric power (mainly diesel), it is desirable from the viewpoint of energy conservation and the environment to generate electricity using this tidal current power.

## III. DESIGN OF TIDAL TURBINE WITH LARGE DIFFUSER

The design of our turbine is based on "wind lens" technology [1], as this has been proven to provide high efficiency for a given turbine rotor blade size. In the case of a wind turbine, the size of the diffuser is generally limited by the high cost of creating a diffuser and tower capable of withstanding typhoon strength winds (in the case Japan), although clearly increased tower height and diffuser size will increase the efficiency of the wind turbine. However, in the case of using a large diffuser underwater, the diffuser provides the buoyancy necessary to counterbalance the weight of the generator, and the occurrence of extreme weather conditions (typhoons etc.) has little affect below the surface at the depth used for power generation, therefore the use of a large diffuser is feasible.

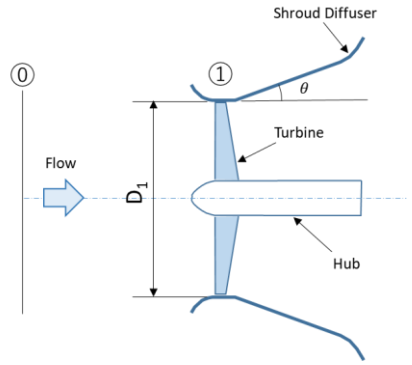


Fig. 3. Meridional section of a horizontal axis tidal current turbine with shroud.

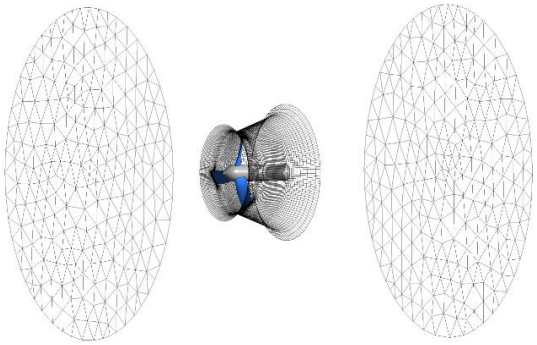

Fig. 4. Computational mesh with a structured mesh for internal of the turbine flow and an unstructured mesh for outer flow of the turbine.

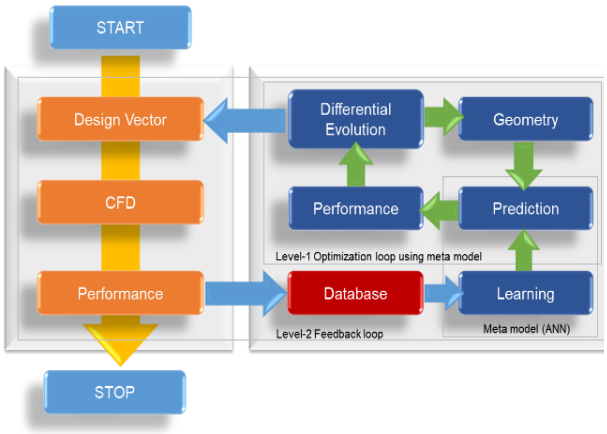


Fig. 5. General layout of the VKI optimization system.

### A. *Target turbine and numerical approach*

An experimental model turbine generator is shown in Fig.3. The baseline turbine has 3 blades with a diameter of D1= 0.3m to match the model experiment, and profile of the blade is based on an NACA4616 aero-foil. The diffuser's combined diameter and profile provides the buoyancy to balance the weight of the submerged turbine generator. Although the interesting physics of the wind lens technology is the brim effect, it is not applied to the simulation of the water lens turbine in this study. As shown in Fig. 4, for the numerical simulation, an inlet boundary is applied as 2.7 times $D_1$ far from the turbine inlet, an outlet boundary is applied as 3.3 times larger

than $D_1$. For the tidal turbine, an artificial diffuser wall with zero thickness is applied for instance generating a numerical mesh. As a general rule in order to generate effective computational mesh an unstructured mesh is used at the outlet and a structured mesh is used at the inlet of a turbine flow.

The steady-state numerical simulations were conducted with ANSYS-CFX 19.1 commercial CFD code. In this study, 70 thousand nodes of unstructured mesh in a stationary domain are generated by ANSYS ICEM-CFD, and 380 thousand nodes of structured mesh in a rotational domain are generated by ANSYS Turbogrid. Each domain is connected by a Frozen Rotor Interface domain. The working fluid is water, and a turbulence model of the SST (Share Stress Turbulence) model was used for the flow with a low Reynolds number of $3\times10^5$. An averaged first cell spacing of y+=20 was used at the internal wall of the diffuser. The axial component of velocity at the inlet boundary is kept at a constant speed of $U_0$=1.0 m/s. The rotational speed of the turbine is adjusted to vary the tip speed ratio $\lambda_0$ as defined in Eq. (1). The output shaft power is normalized as a power coefficient $C_{P0}$ with reference to $A_1$ at the blade inlet as shown in Eq. (2). The power coefficient $C_{P0}$ is defined for the turbine without shroud and it defines the efficiency of the turbine. However, in the case of the current study of the shrouded turbine, the accelerated flow at the turbine inlet $U_1$ varies from $U_0$. It is here we must note that that the power coefficient $C_{P0}$ does not define the efficiency of turbine in the case of the shrouded turbine. The reason the power coefficient $C_{P0}$ is applied in this study is that it is a useful parameter when estimating the output power from varying blade diameters and flow conditions in the tidal flow. The efficiency of the shrouded turbine is discussed in a later section in this paper.

$$\lambda_0 = \frac{D_1 \cdot \omega}{2 \cdot U_0} \tag{1}$$

$$C_{p0} = \frac{Trq \cdot \omega}{0.5 \cdot \rho \cdot A_1 \cdot U_0^3} \tag{2}$$

### B. *Optimization system*

The optimization system used in this research was developed by the von Karman Institute for Fluid Dynamics and it is applied to a variety of turbomachinery applications. The general concept of the optimization system is outlined in Fig.5. The vertical flow from top down on the left represents the traditional design procedure in which theoretical considerations and experimental data plays a crucial role. The upper right box (Level 1) represents the optimization loop comprising of a differential evolution algorithm (DE) and a meta-model based on an Artificial Neural Network (ANN). The ANN replaces the computationally expensive CFD simulations in the optimization loop (Level 1) and provides less accurate but very fast performance predictions to evaluate a large number

TABLE I
DESIGN PARAMETERS FOR OPTIMIZATION

| opt param | Blade Hub | | Min | Max |
|---|---|---|---|---|
| opt-1 | AxialPump.Geo.Blade.Hub.Beta.Point1.Y | deg. | 5 | 15 |
| opt-2 | Delta_HubBeta_12 | deg. | 5 | 15 |
| opt-3 | Delta_HubBeta_23 | deg. | 0 | 10 |
| opt-4 | AxialPump.Geo.Blade.Hub.Meridional.Point2.X | m | 0.024 | 0.036 |
| | BladeMid 1 | | | |
| opt-5 | AxialPump.Geo.Blade.Mid1.Level | - | 0.1 | 0.5 |
| opt-6 | AxialPump.Geo.Blade.Mid1.DeltaTheta.Point1.Y | deg. | 0 | 5 |
| opt-7 | AxialPump.Geo.Blade.Mid1.DeltaTheta.Point2.Y | deg. | -20 | 0 |
| | Blade Shroud | | | |
| opt-8 | AxialPump.Geo.Blade.Shr.Beta.Point1.Y | deg. | 55 | 62 |
| opt-9 | Delta_ShroudBeta_12 | deg. | 0 | 15 |
| opt-10 | Delta_ShroudBeta_23 | deg. | 0 | 5 |
| opt-11 | AxialPump.Geo.Blade.Shr.Meridional.Point2.X | m | 0.009 | 0.015 |
| | Shroud Casing | | | |
| opt-12 | AxialPump.Geo.Meridional.Patch1.Shr.Point1.Y | m | 0.174 | 0.15 |
| opt-13 | AxialPump.Geo.Meridional.Patch3.Shr.Point2.X | m | 0.09 | 0.192 |
| opt-14 | AxialPump.Geo.Meridional.Patch3.Shr.Point2.Y | m | 0.15 | 0.21 |
| opt-15 | Delta_ShroudOuterRadius | m | 0 | 0.036 |

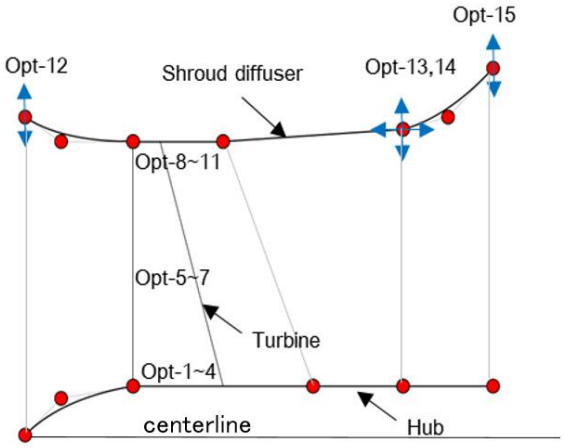


Fig. 6. Control points of design variable for optimization.

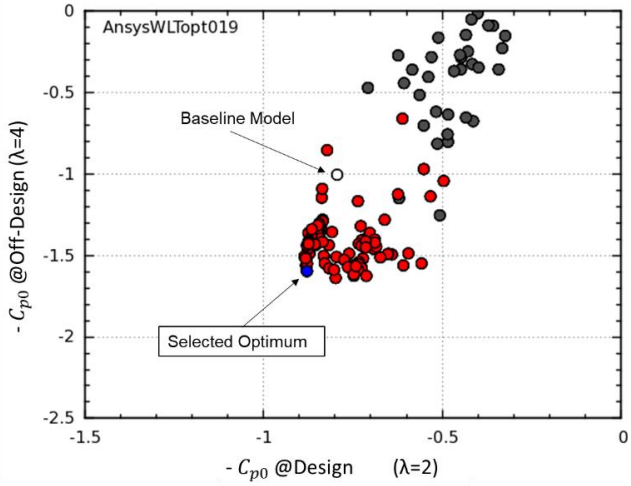


Fig. 7. Optimization result on two objective space.

of geometries using the differential evolution algorithm during its search for the optimum. In order to train the meta-model for prediction, a database is required of previous reliable numerical data.

The database was, therefore, initialized by means of a Design of Experiment (DOE) comprising 64 designs in an advanced optimization loop (Level 1). After building a database and training the meta-model (ANN), the

optimization loop (Level 1) is invoked and DE predicts the optimal geometries. However, ANN requires validation which is then performed in the feedback loop (Level 2). The optimal geometries coming from the ANN prediction are confirmed by the more computationally accurate and expensive CFD calculations to verify the accuracy of the meta-model (Level 2). The results of the more accurate performance analysis are added to the database and a new optimization loop is started based on the additional training of the meta-model and the additional database.

### C. *Objective function and design parameters*

The optimization result is shown in Fig.7 as a dual correlation of both objectives within the same space. The horizontal axis shows the power coefficient $C_{p0}$ for the design tip speed ratio of $\lambda_0$=2.0, and the vertical axis shows the power coefficient at the off-design tip speed ratio of $\lambda_0$=4.0. Each objective is shown as a minimized problem multiplied by -1, the lower left corner of the figure shows the best candidate. The black circles indicate individual resutls from the DOE process for the initial learning of the ANN. The red circles indicate the individual results from the search system GA+ANN. In total 150 individual results are considered during the optimization process of the Level-2 loop as shown in Fig.5. The hyperbolic shape of the front end of the individual results forms a Pareto front, which indicates that the two objective functions are competing (trading-off with each other) and therefor it is difficult to improve both objective functions within the same turbine configuration.

One of the individual results indicated by a red circle is selected as an optimum which is indicated by a blue circle in Fig.7. The selected optimum shows good balance between both objectives.

The upper and lower limit of the design parameters for the optimization are shown in TABLE I. The blade angle and chord length of the turbine blade are varied at the hub and shroud, a point of inflection is introduced to provide a three-dimensional interface to the turbine. As shown in Fig.6, 3 control points (opt-12, 13, 14) for the shroud casing are adopted for varying the conical diffuser length and diameter. The additional parameter of opt-15 provides for a smooth extension at the diffuser's outer perimeter.

### D. *Optimization result*

The optimization result is shown in Fig.7 as a two correlation of the two objectives space. The horizontal axis shows the power coefficient $C_{p0}$ at the design tip speed ratio of $\lambda_0$=2.0, and the vertical axis shows the power coefficient at off-design tip speed ratio of $\lambda_0$=4.0.

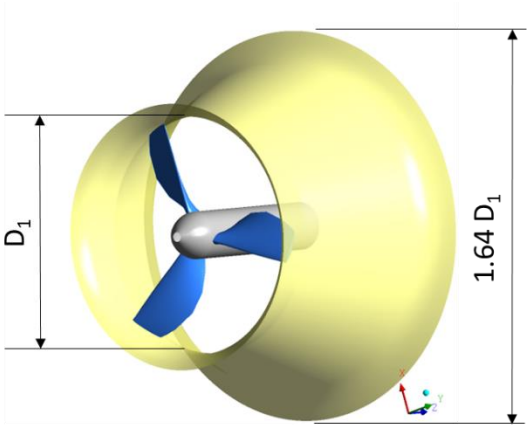


Fig. 8. Optimization blade and shroud.

Fig. 9. Experimental setup of the optimized turbine with the shroud in the circulating water channel.

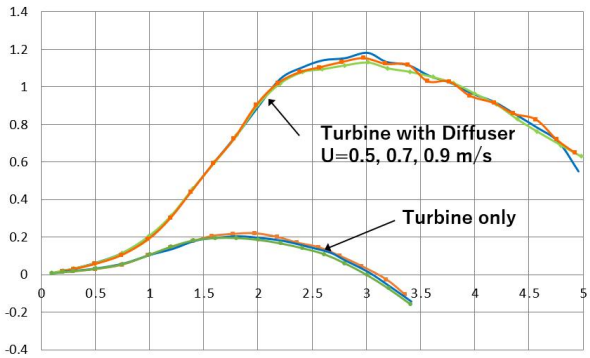


Fig. 10. Experimental results of the power coefficient of the optimized turbine with/without shroud.

Each objective is shown as a minimize problem multiplied by -1, the lower left corner of the figure shows good candidate. The black circles indicate the individuals by the DOE process for the initial learning of the ANN. The red circles indicate the individuals from searching system GA+ANN. Totally 150 individuals are considered during the optimization process of the Level-2 loop as shown in Fig.5. A hyperbolic shape of the front end of the individuals forms a Pareto front, which indicates that two objective functions are under a trade-off condition and it is difficult to improve both objective functions in same configuration of the turbine.

One of individuals of the red circle is selected as an optimum which is indicated by a blue circle in Fig.7. The selected optimum shows good balance for both of objectives.

A three-dimensional rendering of the selected optimum is shown in Fig.8. The outlet diameter of the diffuser is 1.64 $D_1$, which is the maximum size of the diffuser within the range of the design parameters. The turbine blade reflects a three-dimensionally skewed shape. The stagger angle is 15.9 deg. at the hub side, and it is 64.0 deg. at the shroud side.

We conducted performance tests for the optimized turbine with shroud in a circulating water channel shown in Fig.9 at the Research Institute for Applied Mechanics, Kyushu University. The shroud was made with stainless steel and the turbine was 3D printed. The diameter of the turbine was 0.3 m and it was rotated at a number of constant speed ratios by a motor, in steady flow speeds of U=0.5, 0.7 and 0.9 m/s. Here the turbine generator was being driven as a motor and the net torque acting on the motor was measured. The rotational torque acting on the turbine was measured both with and without the shroud.

Fig. 10 shows the results of the power coefficient of the turbine with and without shroud of the tip speed ratio (TSR). We understand that the maximum peaks of the power coefficient of the turbine without shroud are about 0.2 around TSR = 2.0, and about 1.2 at TSR = 3.0 for the turbine with the shroud. This can be explained in that the local flow velocity at the turbine is accelerated by the shroud. In the case of an ordinary turbine (without shroud), the maximum efficiency is about 0.4, so it can be said that this turbine with shroud is three times as efficient. The efficiency based on the optimization calculation was higher than the experimental results, clearly the accuracy of the CFD used in the optimization calculation will define the precision, however the general tendency of the optimization design of the turbine correlates well in the case with the shroud.

## IV. FLOATING/SUBMERSIBLE TIDAL TURBINE SYSTEM

As the tidal power generator is normally installed and operated under sea water, marine work in the sea are necessary, and it is essential to recover and reinstall the tidal power generator for periodic maintenance during long-term operation. As the total weight of a tidal turbine of mega-watt class currently under development is around 1,000 tons, the cost of marine work is very high requiring a large working ship, DPS crane ship or a dedicated ship may be required for installation and recovery, which increases the maintenance cost (OPEX) of the tidal power generation.

We propose a system using rope mooring and floating/submersible type tidal current power generator to minimize the cost for marine work. The method uses the characteristics of tidal current which changes flow direction every 6 hours, and when the tidal current is weak, the tidal power generator floats to the surface and it can be recovered by removing the mooring lines and towing it to port by small boat such as a fishing boat as shown in Fig.11. When the tidal current becomes strong, the device passively submerses below the surface of the water, and power generation becomes possible in the tidal current.

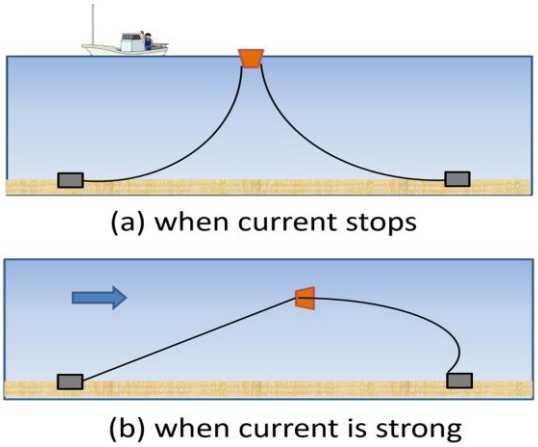


Fig. 11. Mooring system for floating/submersible power generator.

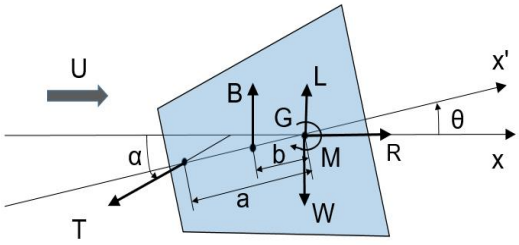


Fig. 12. Definition of force and moment of mooring body.

With reference to Fig.12, the symbols have the following meanings.

G: Center of gravity, W : Weight in air, B : Buoyancy,
T : Tension of rope, U : Flow velocity,
(R, L, M) : Hydrodynamic force/moment of the body including the turbine thrust force
a : Distance from the center of gravity to the mooring point/s
b : Distance from the center of gravity to the buoyancy
$\alpha$: Inclination of mooring line, $\theta$: Trim angle of the body

Writing the equations of equilibrium with respect to G as follows

$$B = T\sin\alpha + W - L \tag{3}$$

$$R(\theta) = T\cos\alpha \tag{4}$$

$$0 = Bb\cos\theta - Ta\sin(\alpha - \theta) + M \tag{5}$$

where R(θ) is resistance of the body including the turbine thrust :

$$R(\theta) = \frac{\rho}{2} AU^2(1 + f(\theta)) \times C_D \qquad (6)$$

where $C_D$: Resistance coefficient including turbine thrust

when the generator faces to the flow then we put θ=0 and L=M=0 from the symmetric relation of the body we obtain the following equation from (4) and (5).

$$b = a \tan \alpha \times {}^{R}/_{B} \qquad (7)$$

where $R = \frac{\rho}{2} AU^2 \times C_D$

That is, in order to position the generator directly into and against the flow, it is necessary to adjust the point of mooring or the centre of buoyancy.

Use SI (MKS) as primary units. Imperial units may be used as secondary units (in parentheses). An exception is when Imperial units are used as identifiers in trade, such as "3½-in pipe." Avoid combining SI and CGS units, such as flow in cm/s. This often leads to confusion because equations do not balance dimensionally. If you must use mixed units, clearly state the units for each quantity in an equation.

## V. MODEL EXPERIMENTS

### A. Experimental model

In order to confirm the feasibility of this proposed mechanism, we made a model which is shown in Fig. 13 and conducted experiments in a towing tank. TABLE II shows the principal dimensions of the model. The diameter of the turbine was 0.16 m and it was 3D printed. Regarding the diffuser, the horizontal wing and the nacelle portion including the inlet and the mooring points were 3D printed, and polystyrene was laminated to the diffuser to provide additional buoyancy.

The experiment was carried out twice: the first experiment was conducted in a circulating water channel (measuring: L x B x d = 6 m x 1.5 m x 1.3 m) at RIAM Kyushu University in July 2017, the second experiment was carried out in a deep towing tank (L x B x d = 65 m x 5 m x 7 m) in October 2017. As the flow is unidirectional in a circulating water channel, the depth and trim of the model in this uniform flow were measured. On the other hand, in the deep towing tank, the towing carriage was driven sinusoidally to approximate the relative flow velocity of a tidal current. The main purpose of the experiment in the towing tank was to confirm whether the model stably changes direction in the sinusoidal flow. For experiments in the deep tank, a false bottom (L x B = 4.5 m x 1.8 m) was set under the towing carriage at 1.2 m below the water surface so that it moved together with the towing carriage.

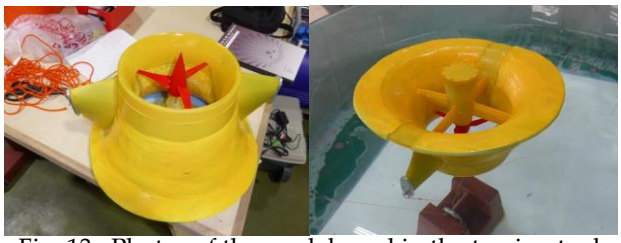

Fig. 13. Photos of the model used in the towing tank experiments.

TABLE II
PRINCIPAL DIMENSIONS OF THE MODEL USED IN THE CIRCULATING WATER CHANNEL AND TOWING TANK EXPERIMENTS

| | | |
|---|---|---|
| Turbin diameter | | 0.16 m |
| Diffuser | Inlet dia | 0.205 m |
| | Exit dia | 0.4 m |
| | Length | 0.22 m |
| Weight in air | | 5.77 kgf |
| Movable weight | | 0.975 kgf |
| Buoyancy | | 77.1 N |
| Center of gravity | | 0.176 m |
| Center of buoyancy | | 0.164 m |

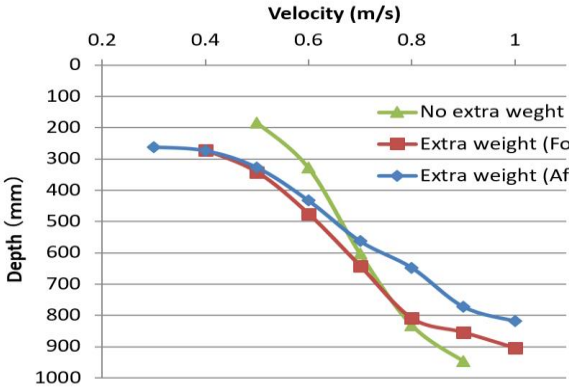


Fig. 14. Depth of the model in flow speed as a function of movable extra-weight condition.

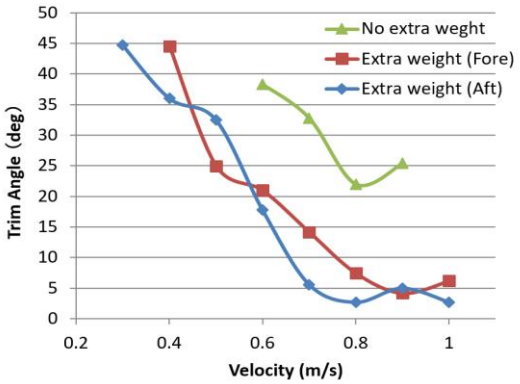


Fig. 15. Trim angle of the model in flow speed as a function of movable extra-weight condition.

### B. Experimental results

In the circulating water channel experiment, the model was visible through glass on the side, allowing video footage to be taken by two cameras to analyze the depth and trim of the model using a 3 dimensional image

tracking system (DippMotionPro). Fig. 14 compares the model depth with and without additional weight (0.975 kg). Also, Fig. 15 compares the trim angle of the model at the same time. From these results, with the additional weight, at low flow speed, it floated with the trailing section facing upward near the water surface, but when the flow velocity became larger than 0.4 m/s, it sank proportionally to the flow speed and the trim angle also decreased. On the other hand, in the absence of additional weight, the depth of the model was almost same, but the trim angle was never less than 20 degrees. The reason for this is presumed from the result of the balancing equation, thus (5) could not be satisfied without additional weight.

In the experiments, the effects of the location of the mooring points on the submerging depth and trim angle of the model were also checked. The mooring points were moved rearward at 10 mm intervals. As a result, the location of the mooring points did not significantly impact the submerging depth, however the trim angle had a considerable effect. In this case, a point located 20 mm behind the initial point proved to be an optimal point.

Next, for the experiment in the tidal flow carried out in the towing tank, the towing carriage was operated sinusoidally for about 180 seconds per cycle in the centre part of the tank. The towing carriage travelled from the ends of the tank so that the maximum speed was 0.8 m/s at the centre part, each experiment was repeated five times to confirm the stability of the measurements. Measurement of the depth and trim angle of the main body of the device was carried out using same system as the circulating water channel experiments.

Fig. 16 is an underwater photograph of the experiment, showing the conditions of the model and the mooring lines at maximum flow velocity. For the mooring line, we used intermediate sinkers and confirmed that the model depth can be adjusted by the intermediate sinker positions. We also conducted experiments in the case where the direction of the mooring line and the direction of the flow differed by about 10 degrees, here the equilibrium position of the model changed, but it was confirmed that the attitude of the model remained stable against the flow at the equilibrium position.

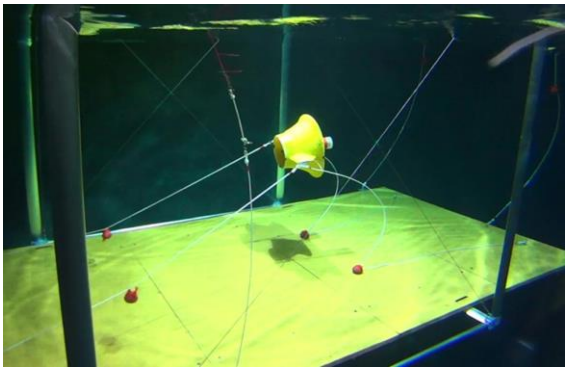

Fig. 16. Photo of the model experiment in the towing tank - false bottom set under the towing carriage.

Finally, regular waves of 1 Hz with about 5 cm in amplitude were generated in the tank to observe the response of the model in a tidal current and waves for the demonstration. When the model approached the water's surface it oscillated slightly with the waves, but it was quite stable. Therefore, from this experiment we can assume that the influence of waves on the surface are not significant.

## VI. CONCLUSION

We propose a floating/submersible tidal current power generation system that can generate electricity with high efficiency by using a large shroud even in sea areas that have lower tidal flow speeds. A search optimization system was applied to the design of a horizontal axis tidal current turbine with shroud using a genetic algorithm. The high performance of the optimized turbine with the shroud obtained was confirmed by scale model experiments.

This system utilizes the regularity of the tidal current, it floats on the water surface when the tidal current stops, and it dives under the water surface and generates power when the tidal current is strong. Since the tidal power generator is loosely moored by four ropes, recovery and re-installation is possible using a small boat (such as a fishing boat) when the tide stops, thereby the cost of offshore work can be minimized. The feasibility of this system was verified by the model experiments.

Currently, we are planning a sea trial of a 5kW larger scale model shown in Fig. 17, and we would like to report on this result in the near future.

## REFERENCES

[1] Y. Ohya and T. Karasudani, "A Shrouded Wind Turbine Generating High Output Power with Wind-lens Technology", *Energies*, vol. 3, pp. 634-639, 2010.

[2] H. Sun, S. Yamaguchi and Y. Kyozuka, Tidal Current Energy Assessment Around Goto Islands, Japan, Proceeding of the International Symposium on Marine and Offshore Renewable Energy (MORE), 1-8, 2013

[3] D. Sakaguchi and Y. Kyozuka, "Global Optimization of a Horizontal Axis Tidal Current Turbine with Shroud" in the proceedings of the 4th AWTEC, 2018.

Fig. 17. A photo of the floating/submersible shrouded tidal current turbine for the demonstration experiment in the Naru Strait in Goto, Nagasaki.